



PERFORMANCES OF METAL OXIDES SUPPORTED IN MONOLITH FOR COMBINED SO₂/NO_x REMOVAL FROM FLUE GAS

S. Kiman*, H. D. Mohammed, N. B. Aliyu, T. H. Usman and D. B. Kayode

Department of Chemical Engineering, University of Maiduguri, Bama Road, PMB 1069 Maiduguri, Borno State, Nigeria

*Corresponding author's email address: silaskiman@unimaid.edu.ng

ARTICLE INFORMATION

Submitted 30 August, 2021
Revised 2 December, 2021
Accepted 2 December, 2021

Keywords:

Adsorption capacity
Fossil fuels
Breakthrough curve
Monolith adsorbent

ABSTRACT

The emission of acid gases such SO₂ and NO_x have detrimental effects on human beings and the environment hence, removing them from flue gas in a dry adsorption process is desirable. In this work, carbon monolith was synthesized with various metals consisting of CeO₂, Co₃O₄, V₂O₅, and CuO by deposition precipitation, hydrothermal and wet pore volume impregnation synthesis techniques. The fixed bed adsorption activity test was carried out with flue gas production by coal burning. Furthermore, the breakthrough curves of the adsorbents were investigated where the adsorbent developed via hydrothermal technique with Co₃O₄ metal oxide termed as HM-Co₃O₄ ICM displayed higher adsorption capacity for both SO₂ (103.9 mg/g) and NO_x and (106.6 mg/g). The Langmuir model can best describe the experimental data based on the correlation coefficient and separation factor results. These results implied that the developed adsorbent can be potentially used in the industry for flue gas cleaning.

© 2022 Faculty of Engineering, University of Maiduguri, Nigeria. All rights reserved.

1.0 Introduction

Nitrogen oxides (NO_x) and sulfur dioxide (SO₂) are pollutants that are produced from fossil fuels which may cause acid rain, depletion of the ozone layer, urban smog, several illnesses, acceleration of the degradation of buildings, monuments, and structures (Rosas *et al.*, 2017; Wu *et al.*, 2016). The apprehension of such pollutants on the environment and human health has motivated a global campaign on strategies to abate their emission (Abdulrasheed *et al.*, 2018). Wet flue gas desulfurization (WFGD) being the evolved matured technology used for SO₂ removal is incapable of eliminating NO_x. Alternatively, Alternatively, selective catalytic reduction (SCR) is widely utilized for the NO_x control but due to catalyst fouling, operating and capital cost, it is limited (Wu *et al.*, 2016). Therefore, the development of a cost-effective method for combined NO_x/SO₂ removal is desirable.

It was reported that the removal of acidic gases in flue gas composition by adsorption has advantages such as high removal efficiency, selectivity, regeneration potential with the simplicity of design and operation (Abdulrasheed *et al.*, 2018). Also, adsorption is one of the most promising methods for pollutants abatement, however, however, the adsorbent and supported active species are critical to the adsorptive performance (Yin *et al.*, 2018). The supporting material must be characterized by high surface area, pore structure, and abrasion resistance moreover, the dispersion of the metallic components can promote the catalytic properties on the support (El-Khouly *et al.*, 2017). Kiman *et al.* (2018) found that monolith has the required surface area, attrition, and fly ash plugging resistance, therefore, it can be used in heterogeneous catalysis as support. However, Mo *et al.* (2018) stated that the dispersion of active components on the monolith is always in-homogeneous and easy to aggregate during impregnation and therefore has a negative effect on practical use. Therefore, some efforts must be devoted to growing nanoarray-based catalysts on channeled monolithic substrates to promote catalytic activity.

The surface chemistry of an adsorbent can affect its adsorption and catalytic abilities (Sousa *et al.*, 2018) while the surface functional groups of the support played a significant role in determining the extent of interaction with the active precursor during adsorbent preparation (Ibraheem *et al.*, 2014). Hence, the introduction of hetero elements such as Co_3O_4 , $\text{Ni V}_2\text{O}_5$, Ce, and CuO on the adsorbents can significantly improve the catalytic activity (Cui *et al.*, 2018; Ibraheem *et al.*, 2014).

The objectives of this study are to synthesize monolith adsorbents by deposition precipitation, hydrothermal and wet pore volume impregnation synthesis techniques with various metal oxides, and the breakthrough study of the adsorbents through the combined NO_x/SO_2 removal from flue gas. The adsorbent with highest adsorption capacity was investigated by FTIR, BET surface area, SEM and EDX analysis, isotherm study, optimization of independent variables in adsorption with RSM software and the regeneration potential of the adsorbent.

2. Materials and Methods

2.1. Materials

The monolith used has a channel of 1.02mm and a wall thickness of 0.25mm. Urea ($\text{CH}_4\text{N}_2\text{O}$), nitrate hexahydrates ($\text{X}(\text{NO}_3)_2 \cdot 6\text{H}_2\text{O}$), and nitric acid (HNO_3 , 65%), were purchased from Beihai Huijiang Chemical China. The chemicals and reagents used were all of analytical grade.

2.2 Preparation and synthesis of the adsorbent

The monolith structure was carbonized in a horizontal furnace (SA-A35014, Malaysia) by heating at a rate of 5°C min^{-1} up to 800°C for 4 h and in inert condition following activation in CO_2 flow at 350°C for 2 h to obtain carbon monolith (CM). The CM is immersed in HNO_3 for 24 h next it was filtered and washed with distilled water before being placed in a vacuum oven at 70°C and 24 h to dry.

250 mL of deionized water, CM support metal nitrate, and substrate were charged into a reactor vessel of 350 mL capacity while the pH of the solution was made to 3.5 with HNO_3 and heated to 90°C then a solution of urea was added and further heated for 18 h while stirring at 300 rpm. The substrate was filtered, severally washed, and dried at 120°C for 24 h. Finally, it was calcinated in inert at 500°C for 4 h using a heating rate of 5°C min^{-1} . The adsorbent using the deposition precipitation technique is termed DP/CM.

Initially, the metal nitrate hexahydrates precursor and urea ($\text{CH}_4\text{N}_2\text{O}$) were dissolved into a homogeneous solution with 80 mL deionized water under and stirred with the CM. the mixture was charged into 100mL Teflon stainless steel. The autoclave was sealed and reacted at 100°C for 5 h, then it was allowed to cool to room temperature. The samples were washed and ultrasonication before drying at 80°C for 2 h. The active metal component catalysts with the CM were heated to 300°C for 2 h at a heating rate of 3°C min^{-1} . The hydrothermally synthesized technique adsorbent is termed HM/CM.

An aqueous solution with the metal nitrate precursor was mixed with the CM and heated at 70°C with constant stirring (300 rpm) to allow the entire solution to completely evaporate, it was washed and dried at 110°C for 24 h. The CM was annealed at 500°C for 4 h and a heating rate of 5°C min^{-1} . The adsorbent from the pore volume wetness impregnation technique is termed IM/CM.

2.3 Fixed bed adsorptive test

In the experiment, 1g of the adsorbent was charged into the fixed bed reactor (Figure 1) and firstly preheated in inert for 1h at 100°C . Flue gas was produced in a vertical furnace at 850°C by coal combustion since the industrial flue gas is produced in a power plant furnace at an operating temperature of $>800^\circ\text{C}$ (Li *et al.*, 2008). The generated flue gas was channeled to the adsorbent at 450 mL/min and a

temperature of 150 °C. The inlet and outlet concentrations of NO_x and SO₂ were measured with a T-350 flue gas analyzer. The adsorbent activity test was evaluated through the adsorption capacity as defined by the weight of NO_x and SO₂ captured from the flue gas per gram of adsorbent. The experimental run was performed in duplicate and only the average value was used.

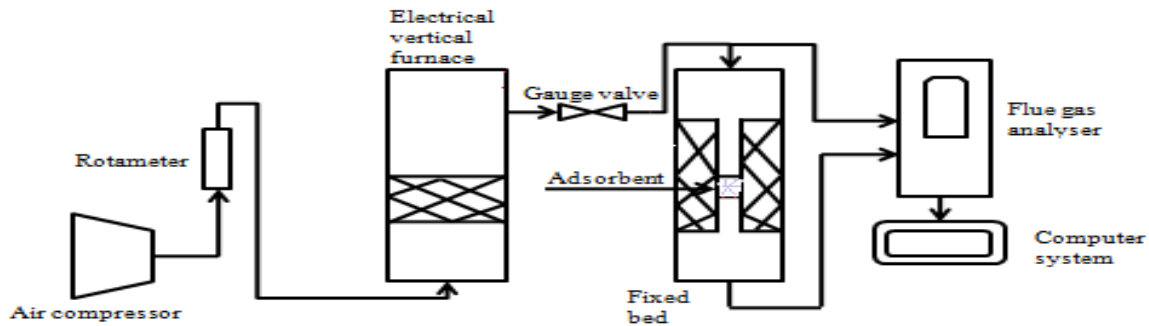


Figure 1: Schematic of the fixed bed adsorption system

2.4 Adsorption isotherm studies

In this work, the equilibrium adsorption data were fitted in Langmuir and Freundlich models. The Langmuir model describes the monolayer adsorption that occurs on the adsorbent surface without interaction among the adsorbed molecules while the Freundlich isotherm is defining multilayer adsorption where the non-uniform distribution of adsorption heat and affinities on heterogeneous adsorbent surfaces occurs (Singh et al., 2018). The adsorption capacity (q_e) in mg/g is given by Langmuir isotherm and presented as (Yi et al., 2012):

$$q_e = \frac{q_m \cdot K_L \cdot C_e}{1 + K_L \cdot C_e} \quad (1)$$

Where C_e is concentration, q_m is the maximum adsorption capacity in mg/g and K_L is the Langmuir constant in L/g, respectively.

The separation factor (R_L) indicates Langmuir isotherm suitability (favorable; $0 < R_L < 1$):

$$R_L = \frac{1}{1 + K_L \cdot C_0} \quad (2)$$

where C_0 initial concentration in mg/L.

The Freundlich model is (Yi et al., 2012):

$$q_e = k_f C_e^{1/n} \quad (3)$$

where, k_f and n are Freundlich constants (intercept and slope) and the heterogeneity factor.

The linearized form of Langmuir and Freundlich isotherms are (Sharma et al., 2017):

$$\frac{C_e}{q_e} = \frac{1}{q_m K_L} + \frac{C_e}{q_m} \quad (4)$$

and

$$\log q_e = \log k_f + 1/n C_e \quad (5)$$

2.4 Adsorbent characterization

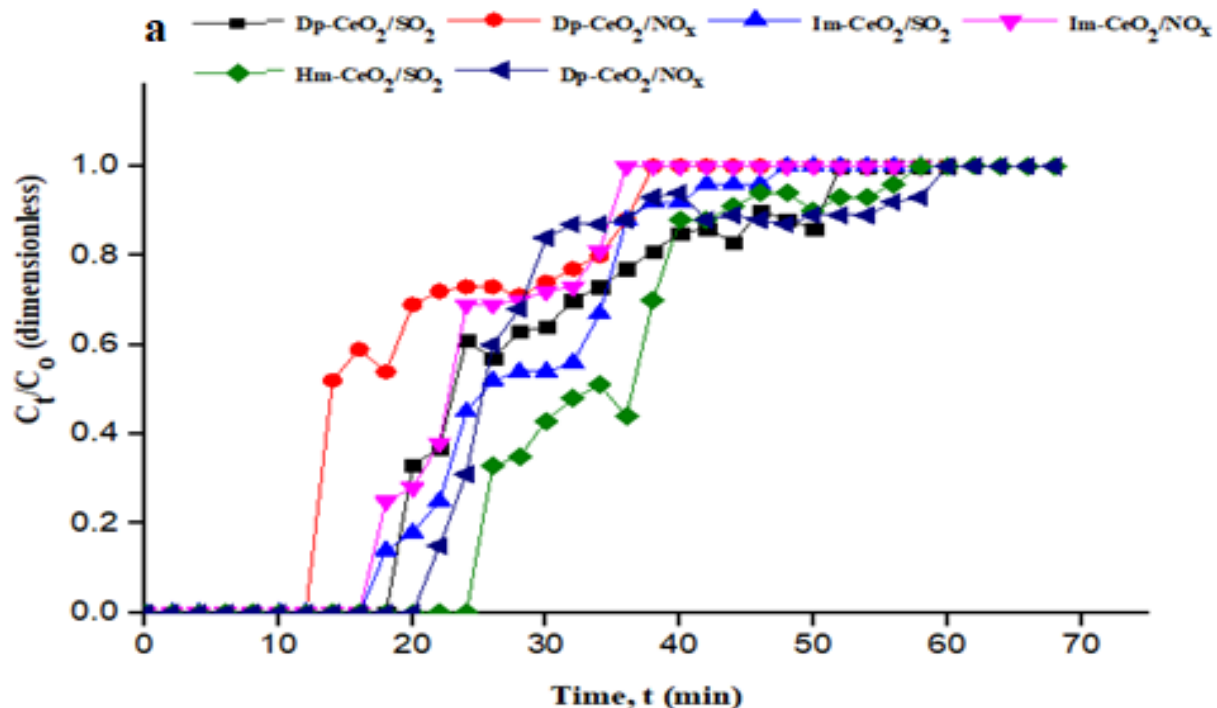
The N₂ adsorption/desorption isotherm was measured with Micrometrics ASAP2020 instrument. Initially, the samples were outgassed at 200 °C for 4 h in the presence of N₂. The isotherms were utilized in calculating the specific surface area S_{BET} . The Fourier transform infrared spectroscopy (FTIR) was used to investigate the functional group attached to the surface of the adsorbent. The infrared spectra of synthesized adsorbent were mixed with KBr and the transmittance mode was verified between 4000 cm⁻¹ and 400 cm⁻¹ with a resolution of 4 cm⁻¹, using a Thermo NicoletAES0200682. Scanning electron microscope with energy dispersive X-ray micro-analyzer (SEM/EDX) (Hitachi Co., Japan, Model No. S3400N) was used to study the morphology of the adsorbent.

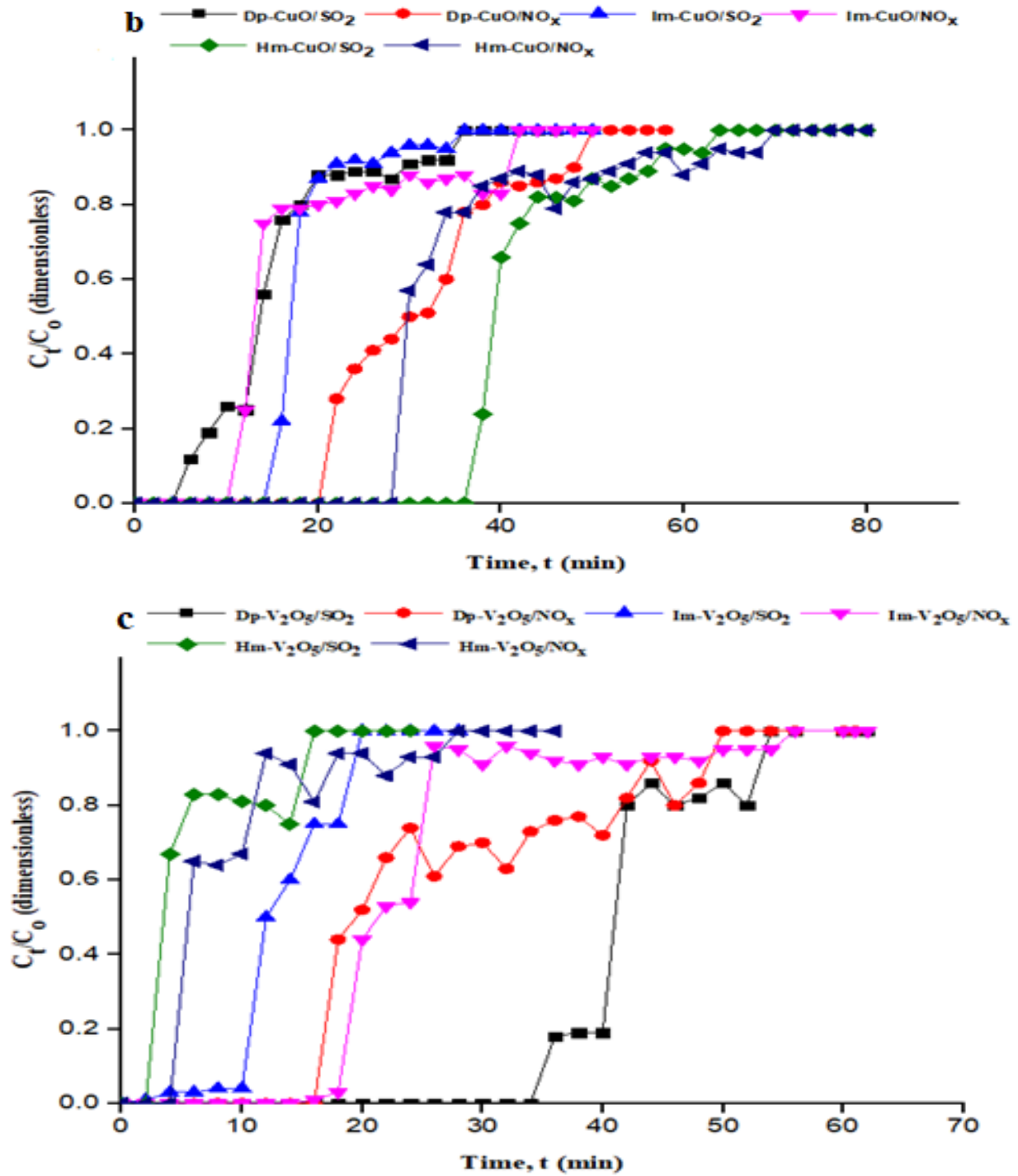
3. Results and Discussion

3.1. Breakthrough curves for various adsorbents

The breakthrough curves were plotted from average experimental values while the performance in terms of adsorption capacity for each adsorbate was evaluated. Figure 2(a-d) shows the breakthrough curves for the combined NO_x/SO₂ removal for the various adsorbents developed.

The CeO₂-based adsorbents in Figure 2a demonstrate 100% initial NO_x/SO₂ adsorption while the hydrothermal synthetic method exhibit a longer breakthrough time about both NO_x and SO₂.





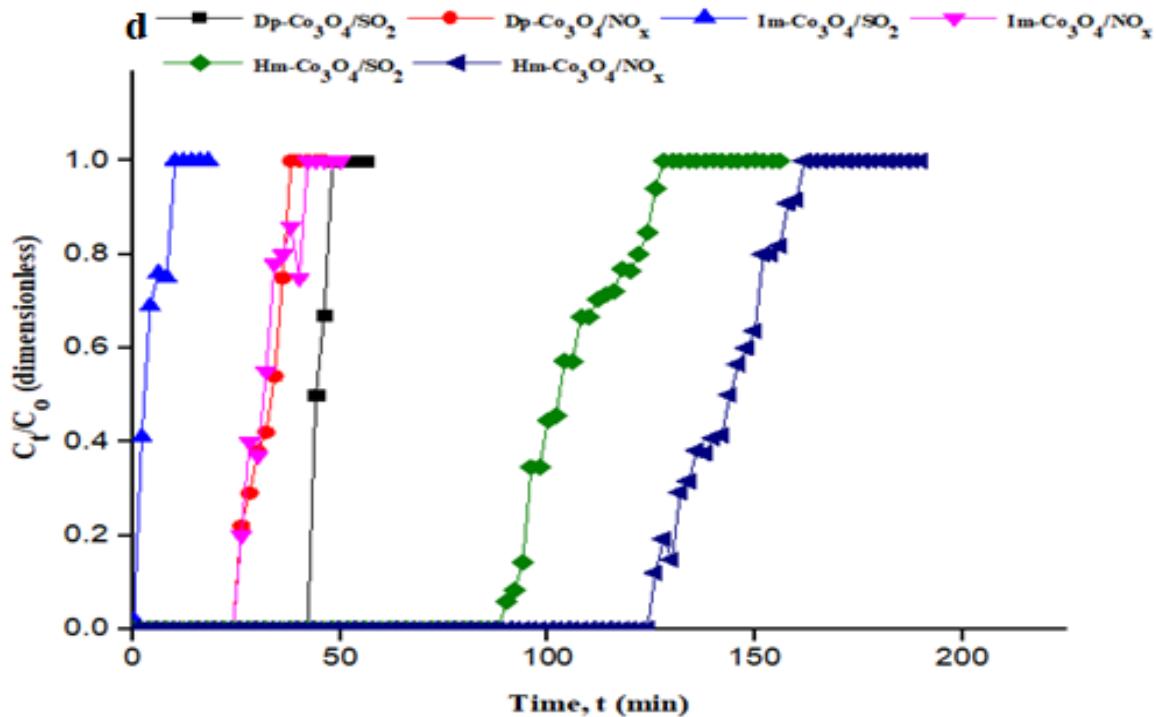


Figure 2: Breakthrough curves of (a) CeO_2 -based (b) CuO -based (c) V_2O_5 -based and (d) Co_3O_4 -based adsorbents.

However, the breakthrough and the saturation times were longer for SO_2 over NO_x and the CeO_2 plays an important role in the NO_x/SO_2 removal. The presence of oxygen surface groups might have increased the t_b because CeO_2 possessed oxidizing property and this fact may indirectly lower the conversion of NO_x (Sumathi *et al.*, 2010a).

The hierarchy of breakthrough time displayed by the CuO -based adsorbent follows as: $\text{HM-CeO}_2/\text{SO}_2 > \text{HM-CeO}_2/\text{NO}_x > \text{DP-CeO}_2/\text{NO}_x > \text{IM-CeO}_2/\text{SO}_2 > \text{IM-CeO}_2/\text{NO}_x > \text{DP-CeO}_2/\text{SO}_2$. Copper based catalysts are known to have high reactivity for SO_2 removal and high catalytic activity for NO_x reduction in its oxide form (Hu *et al.*, 2001). It is assumed that the simultaneous SO_2/NO_x removal occurred for these reasons (Figure 2b). Meanwhile, pores may be blocked which leads to reduced adsorbent performance depending on the synthesis method and compatibility with the metal oxide catalyst.

The presence of SO_2 in the flue gas reduces the adsorbent performance and longevity Garci-Bordeje *et al.*, (2004) but from Figure 1c, V_2O_5 has shown high SO_2 uptake at stack temperatures and the overall performance of the V_2O_5 based adsorbent showed higher SO_2 adsorption compared to NO_x . The role of V_2O_5 in the higher SO_2 removal consists of four steps as follows: the adsorption of SO_2 at sites adjacent to V_2O_5 , the interaction of SO_2 with V_2O_5 to form an intermediate with a structure like VOSO_4 , the reactions of O_2 with the VOSO_4 -like species to yield V_2O_5 and SO_3 and finally, the migration of SO_3 or H_2SO_4 formed between SO_3 and H_2O to the adjacent ACM pores. The former authors reported similar findings (Ma *et al.*, 2008).

Tricobalt tetraoxide (Co_3O_4) has attracted lots of concern because it is cost-effective, has environmental benignity and has good catalytic activity at low temperatures (Mo *et al.*, 2018). The noticeable difference between the HM, DP, and IM methods of synthesis with the Co_3O_4 is shown by the Co_3O_4 -based adsorbents of Figure 2d. The HM method demonstrates outstanding performance in the combined

NO_x/SO₂ removal. This performance suggested that there is uniform dispersion of the Co₃O₄ on the CM. Further, it implies that the hydrothermal treatment and the monolith support used with respect to Co₃O₄ catalyst have a great effect on the adsorption performance. The HM synthesis method also influences the catalytic activity according to previous authors (Radwan et al., 2007).

Initially, there was no 100% SO₂ removal by the IM/CM adsorbent in all of Figure 2, similar findings are reported in previous works (Ghorai and Pant, 2005; Zhou et al., 2012). The highest performance is shown by the HM/CM adsorbent regarding *q*, *t_b* and *t_{sat}* when compared to the Co₃O₄-based adsorbents. Figure 3a illustrates the adsorption capacity of the adsorbents and Figure 3b shows the breakthrough and saturation times of the adsorbents. It can be observed that the highest point is at 130.2 mg/g for *q*-NO_x and for the HM-Co₃O₄/CM adsorbent while the lowest point is shown at 3.1 mg/g for *q*-SO₂ and for HM-V₂O₅/CM adsorbent.

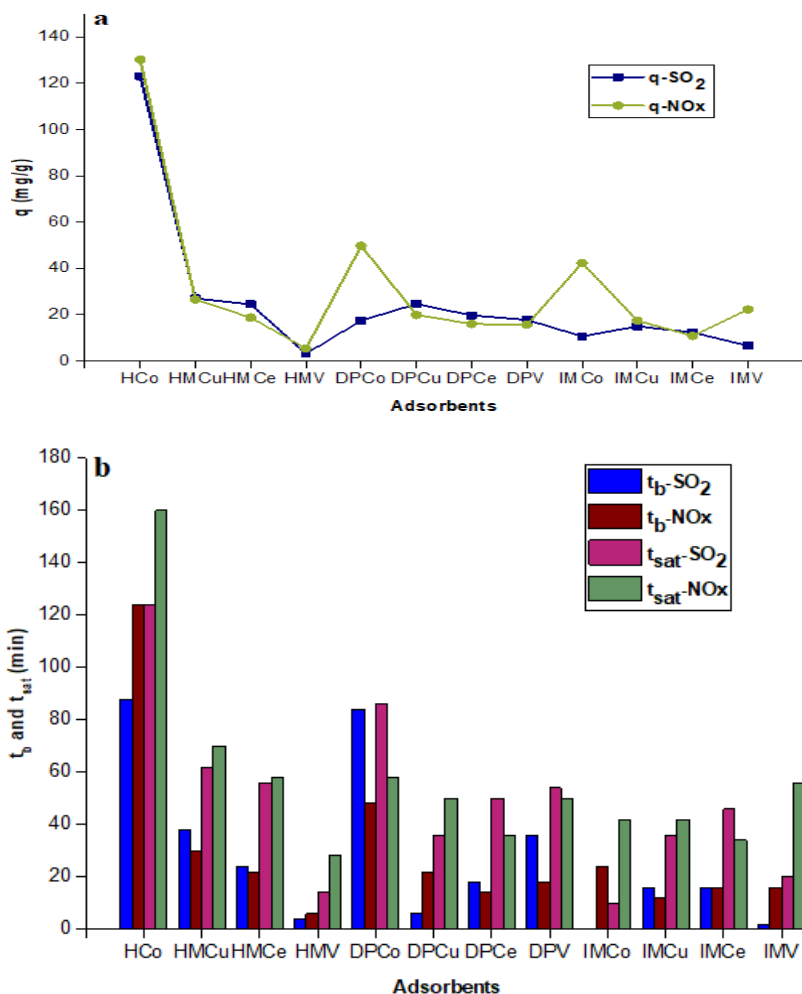


Figure 3: (a) Adsorption capacity measurement (b) Breakthrough and saturation times of the adsorbents.

The demonstration of the HM-Co₃O₄/CM adsorbent to perform in practical application beyond the other adsorbents is because of the compatibility of the adsorbent surface with the Co₃O₄ metal oxide. Furthermore, the result shows how well the hydrothermal synthesis disperses the Co₃O₄ on the support. Meanwhile, the adsorption capacity can be seen to be much favorable towards NO_x adsorbate. The adsorbent's demonstration of high NO_x adsorption affinity is majorly due to the NO_x concentration in the flue gas (Sumathi et al., 2010b; Galvez et al., 2005), the preparation route (Lazaro et al., 2008; Hosseini et al., 2016; Kreutzer et al., 2001), temperature (Sumathi et al., 2010a; Zhao et al., 2011), the oxygen

present (Zhang *et al.*, 2006; Liu and Shih, 2006) and relative humidity (Sumathi *et al.*, 2010b; Dahlan *et al.*, 2009) inactivity test. Figure 3b displayed the time taken for the breakthrough to happen and the saturation time for each adsorbate respectively. The HM-Co₃O₄/CM adsorbent is picked for further studies including characterization, isotherm and RSM optimization.

3.2 HM- Co₃O₄/CM surface area and functional groups

It is revealed in Figure 4a that the adsorbent is of IV isotherm type based on IUPAC classification, suggesting the dominance of mesoporous in the sample. A similar sample of carbon-coated monolith was reported previously (Hosseini *et al.*, 2015). From the BET analysis of the surface area, the surface area is 47.9 m²/g.

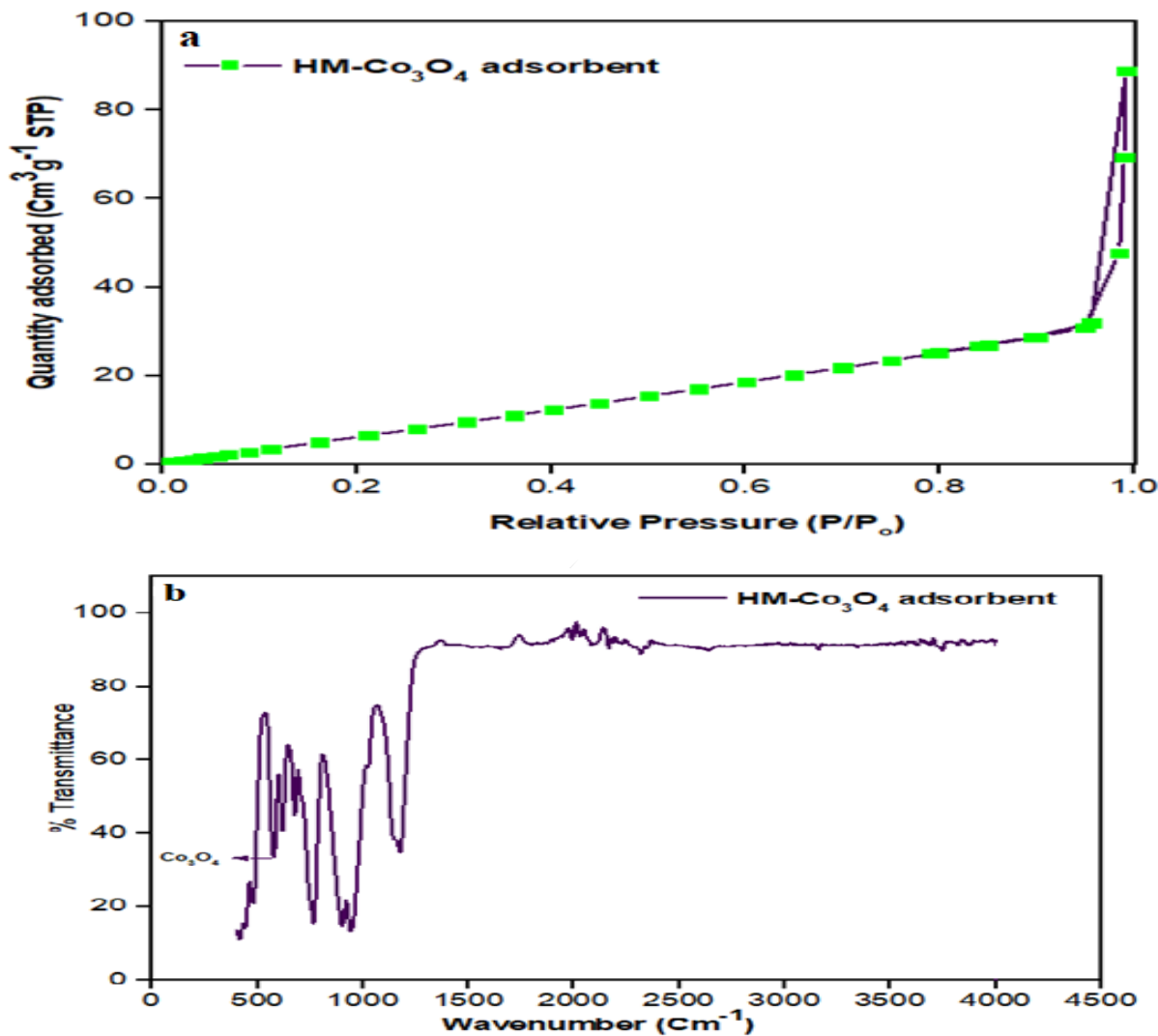


Figure 4: The (a) N₂ adsorption-desorption plot (b) FTIR spectrum of HM-Co₃O₄/CM adsorbent.

The FTIR spectrum in Figure 4b showed several bands belonging to the function groups that are attached on the adsorbent's surface. At 2627 cm⁻¹ there is band ascribed to O-H of carboxylic acid while 2335-2361 cm⁻¹ is ascribed to C-N triple bond. Also, at 1741 cm⁻¹ the C=O of ester stretch was observed, 1370 cm⁻¹ (C-O of a phenolic stretch). Also, assigned to C-O, C-H, CH=CH₂ stretches are the absorption bands at 1175-440 cm⁻¹ (Raghunath and Mondal, 2017; Malkoc *et al.*, 2006). The absorption peaks at 675cm⁻¹-576cm⁻¹ are ascribed to Si-O stretching bands and indicate the presence of Co₃O₄ (Dahlan *et al.*, 2009; Li *et al.*, 2011; Teoh *et al.*, 2013).

3.3 HM- Co₃O₄/CM morphology results

The surface morphology and elements of the HM-Co₃O₄/CM adsorbent are presented in Figure 5.

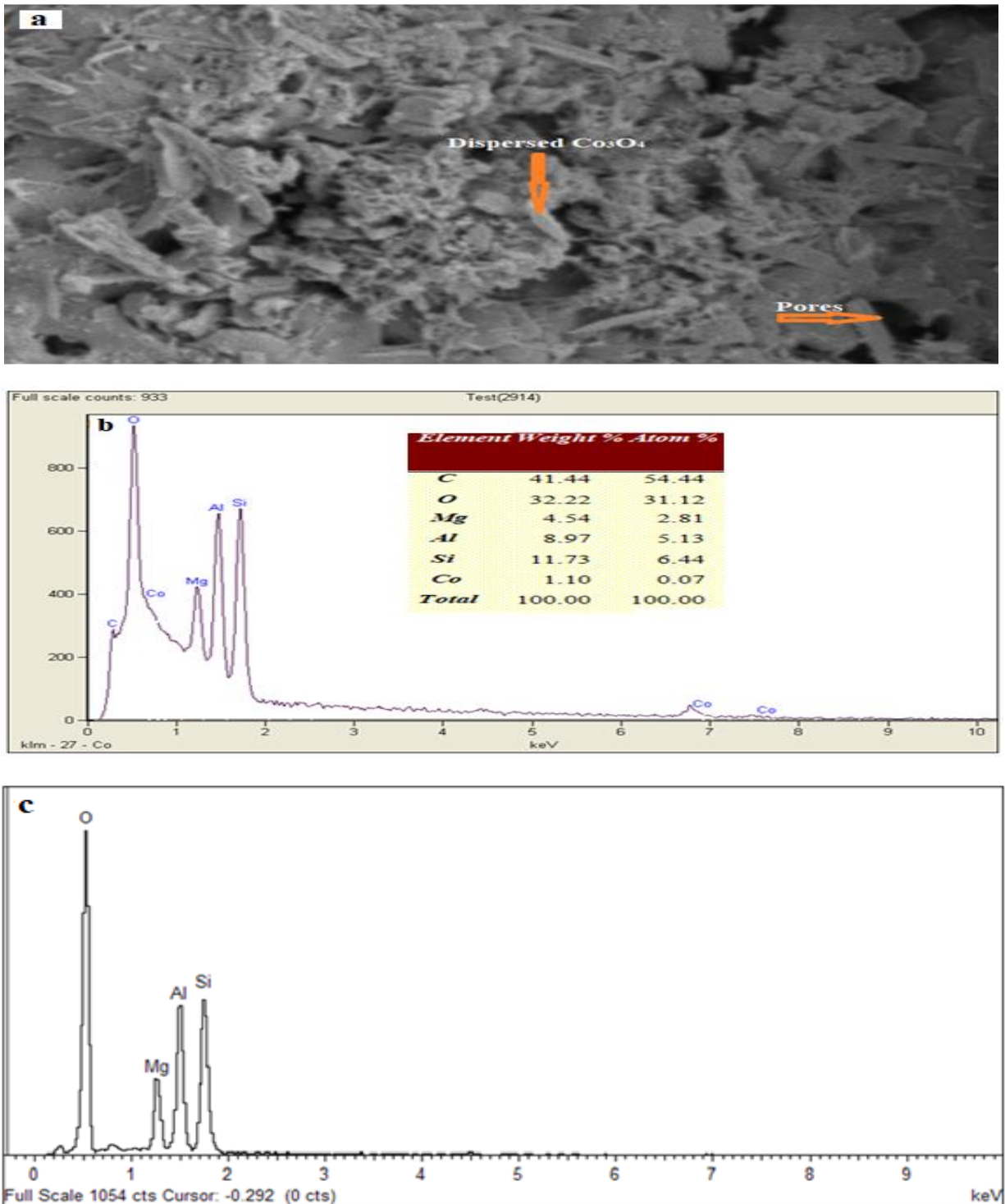


Figure 5: (a) SEM microphotographs (b) Elemental result and (c) EDX peaks

In Figure 5a, the surface structures by SEM illustrates the uniform dispersion of the Co₃O₄ catalyst on the CM surface area in a rich spider-like web, similar microphotograph was previously presented (Sumathi et al., 2009). Furthermore, the cordierite has a surface with many large pores which are available for the adsorption to take place. The EDX spectra in Figure 5b showed the presence of Co₃O₄ (1.1%) in the

impregnated CM by EDX techniques. The bare cordierite is made up of Si, Al, O and MgO however, the carbonization process is responsible for the presence of carbon of up to 41.4% by weight which results in the improvement of highly porous surface (Hosseini *et al.*, 2011).

3.4 The isotherms

From Figures 6 a-d, the higher correlation coefficient (r^2) was obtained from the Langmuir model which suggested that the experimental data can be best described by the Langmuir model when compared to the Freundlich model which displayed the r^2 of 0.6682 and 0.8734 for SO_2 and NO_x respectively.

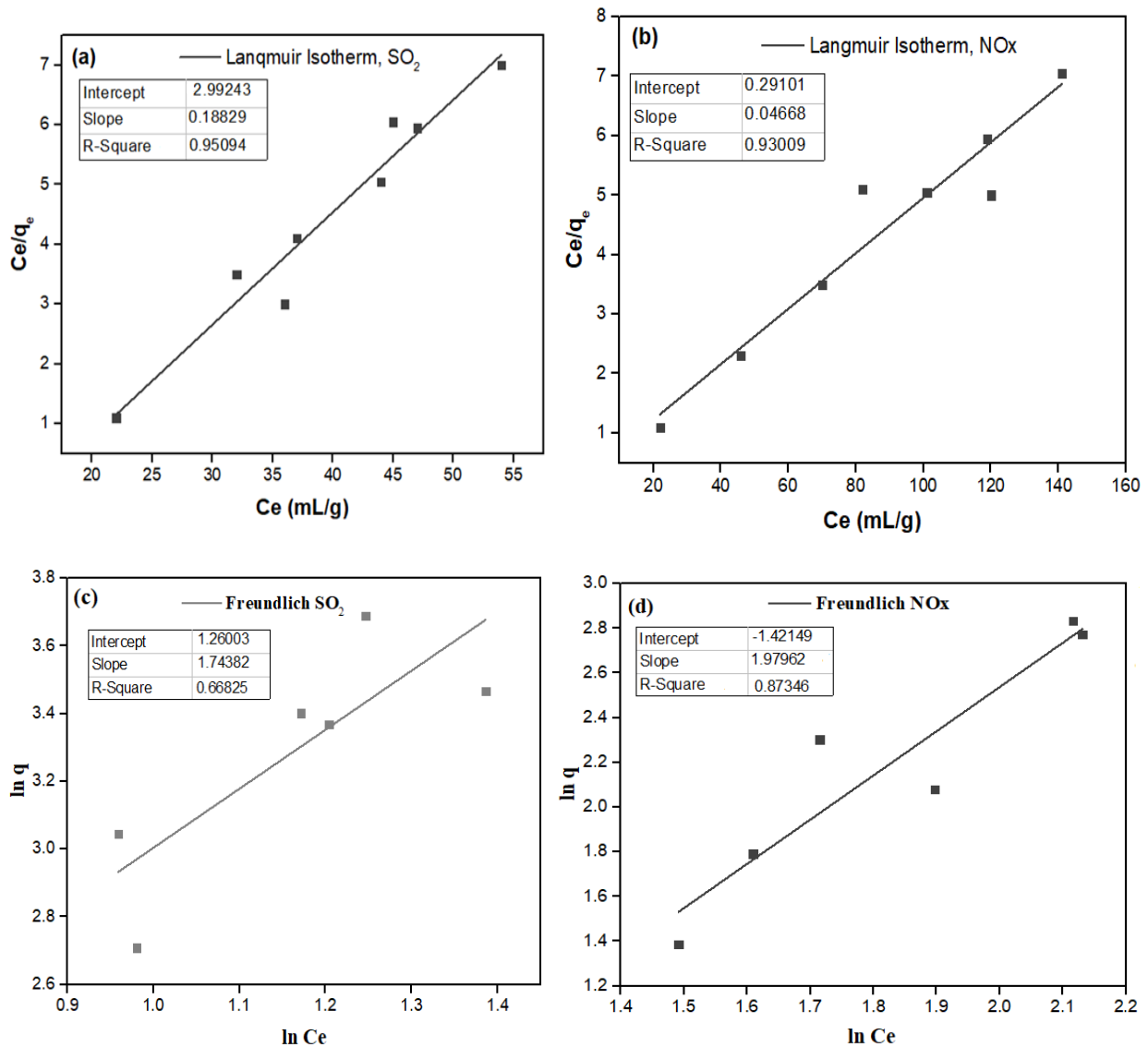


Figure 6: (a) Langmuir isotherm for SO_2 (b) Langmuir isotherm for NO_x (c) Freundlich isotherm for SO_2 and (d) Freundlich isotherm for NO_x .

The r^2 and the parameters for Langmuir and Freundlich models are presented in Table I. Moreover, the R_L value further indicates the suitability of the Langmuir model (0.3377 and 0.0973 for SO_2 and NO_x). The range of favorable adsorption based on the Freundlich model is within the range $1 < n < 10$ (Hosseini *et al.*, 2011). The values for heterogeneity factor for both SO_2 and NO_x are well below the range of favorable adsorption as shown in Table I.

Table 1. The Langmuir and Freundlich parameters results.

q (mg/g) SO ₂ /NO _x	Langmuir parameter	SO ₂	NO _x	Freundlich parameter	SO ₂	NO _x
121.1	q _m	20.0	20.4	k _f	1.26	-1.42
and	k _L	0.344	3.45	n	0.7936	0.7042
130.2	r ²	0.9509	0.9300	r ²	0.6682	0.8734

4. Conclusion

The adsorption capacity of various adsorbents that were impregnated with metal oxides and using three different synthesis methods was studied. By coal combustion in a vertical furnace, flue gas was produced to simulate the generation of flue gas from power plants and the activity test was performed. Meanwhile, the breakthrough curve of combined NO_x/SO₂ was reported. Based on the regression coefficient and the favorable separation factor, the Langmuir model can best describe the experimental data. According to characterization results of the adsorbent with the highest adsorption capacity (HM-Co₃O₄/CM), there is an available active site for the adsorption to occur, the presence of Co₃O₄ was shown.

References

- Abdulrasheed, AA., Jalil, AA., Triwahyono, S., Zaini, MAA., Gambo, Y. and Ibrahim, M. 2018. Surface Modification of Activated Carbon for Adsorption of SO₂ and NO_x: A Review of Existing and Emerging Technologies. *Renewable Sustainable Energy Reviews*, 94(2): 1067–1085. <https://doi.org/10.1016/j.rser.2018.07.011>
- Cui, X., Yi, H., Tang, X., Zhao, S., Yang, K., Yan, B. and Ma, Y. 2018. Study of the Properties of Adsorption of SO₂ – Thermal Regeneration Cycle of Activated Coke Modified by Oxidization. *Journal of Chemical Technology and Biotechnology*, 93: 720–729. <https://doi.org/10.1002/jctb.5421>
- Dahlan, I., Lee, KT., Kamaruddin, AH. and Mohamed, AR. 2009. Selection of Metal Oxides in the Preparation of Rice Husk Ash (RHA)/CaO Sorbent for Simultaneous SO₂ and NO Removal. *Journal of Hazardous Materials*, 166(2-3): 1556–1559. <https://doi.org/10.1016/j.jhazmat.2008.12.028>
- El-Khouly, SM., Mohamed, GM., Fathy, NA. and Fagal, GA. 2017. Effect of Nanosized CeO₂/ZnO Loading on Adsorption and Catalytic Properties of Activated Carbon. *Adsorption Science and Technology*, 35(9-10): 1-15. <https://doi.org/10.1177/0263617417698704>
- Gálvez, ME., Lázaro, MJ. and Moliner, R. 2005. Novel Activated Carbon-Based Catalyst for the Selective Catalytic Reduction of Nitrogen Oxide. *Catalysis Today*, 102–103: 142–147. <https://doi.org/10.1016/j.cattod.2005.02.020>
- García-Bordejé, E., Calvillo, L., Lázaro, MJ. and Moliner, R. 2004. Study of Configuration and Coating Thickness of Vanadium on Carbon-Coated Monoliths in the SCR of NO at Low Temperature. *Industrial Engineering Chemistry Research*, 31(4): 4073–4079. <https://doi.org/10.1021/ie0498854>
- Ghorai, S. and Pant, KK. 2005. Equilibrium, Kinetics and Breakthrough Studies for Adsorption of Fluoride on Activated Alumina. *Separation and Purification Technology*, 42: 265–271. <https://doi.org/10.1016/j.seppur.2004.09.001>

Hosseini, S., Khan, MA., Malekbala, MR., Cheah, W. and Choong, TSY. 2011. Carbon Coated Monolith, a Mesoporous Material for the Removal of Methyl Orange from Aqueous Phase: Adsorption and Desorption Studies. *Chemical Engineering Journal*, 171: 1124–1131. <https://doi.org/10.1016/j.cej.2011.05.010>

Hosseini, S., Marahel, E., Bayesti, I., Abbasi, A., Chuah Abdullah, L. and Choong, TSY. 2015. CO₂ Adsorption on Modified Carbon Coated Monolith: Effect of Surface Modification by using Alkaline Solutions. *Applied Surface Science*, 324: 569–575. <https://doi.org/10.1016/j.apsusc.2014.10.054>

Hosseini, S., Rashid, SA., Abbasi, A., Babadi, FE., Abdullah, LC. and Choong, TSY. 2016. Effect of Catalyst and Substrate on Growth Characteristics of Carbon Nanofiber onto Honeycomb Monolith. *Revista Mexicana De Urologia*, 76: 440–449. <https://doi.org/10.1016/j.jtice.2015.07.015>

Hu, Z., Srinivasan, MP. and Ni, Y. 2001. Novel Activation Process for Preparing Highly Microporous and Mesoporous Activated Carbons. *Carbon*, 39(6): 877–886. [https://doi.org/10.1016/S0008-6223\(00\)00198-6](https://doi.org/10.1016/S0008-6223(00)00198-6)

Ibraheem, NK., Raouf, SR. and Naser, ZA. 2014. Removal of SO₂ Over Modified Activated Carbon in Fixed Bed Reactor: Effect of Metal Oxide Loadings and Acid Treatment. *Iraqi Journal of Chemistry and Petroleum Engineering*, 15(4): 25–35.

Kiman, S., Azlina, GW, Thomas, C. and Umer, R. 2018. Carbonaceous Materials Modified Catalysts for Simultaneous SO₂/NO_x Removal from Flue Gas: A Review. *Catalysis Reviews*, 61(1): 1–28. <https://doi.org/10.1080/01614940.2018.1482641>

Kreutzer, MT., Du, P., Heiszwolf, JJ., Kapteijn, F. and Moulijn, JA. 2001. Mass Transfer Characteristics of Three-Phase Monolith Reactors. *Chemical Engineering Science*, 56(21-22): 6015–6023. [https://doi.org/10.1016/S0009-2509\(01\)00271-8](https://doi.org/10.1016/S0009-2509(01)00271-8)

Lázaro, MJ., Boyano, A., Gálvez, ME., Izquierdo, MT., García-Bordejé, E., Ruiz, C. and Moliner, R. 2008. Novel Carbon Based Catalysts for the Reduction of NO: Influence of Support Precursors and Active Phase Loading. *Catalysis Today*, 137(2-4): 215–221. <https://doi.org/10.1016/j.cattod.2007.11.007>

Li, J., Kobayashi, N. and Hu, Y. 2008. The Activated Coke Preparation for SO₂ Adsorption by using Flue Gas from Coal Power Plant. *Chemical Engineering Process: Process Intensification*, 47(1): 118–127. <https://doi.org/10.1016/j.cep.2007.08.001>

Li, Y., Zhao, J., Dan, Y., Ma, D., Zhao, Y., Hou, S. and Wang, Z. 2011. Low Temperature Aqueous Synthesis of Highly Dispersed Co₃O₄ Nanocubes and their Electrocatalytic Activity Studies. *Chemical Engineering Journal*, 166(1): 428–434. <https://doi.org/10.1016/j.cej.2010.10.080>

Liu, CF. and Shih, SM. 2006. Effects of Flue Gas Components on the Reaction of Ca(OH)₂ with SO₂. *Industrial Engineering and Chemical Research*, 4(26): 8765–8769. <https://doi.org/10.1021/ie0605534>

Ma, J., Liu, Z., Liu, Q., Guo, S., Huang, Z. and Xiao, Y. 2008. SO₂ and NO Removal from Flue Gas over V₂O₅/AC at Lower Temperatures - Role of V₂O₅ on SO₂ Removal. *Fuel Processing Technology*, 89(3): 242–248. <https://doi.org/10.1016/j.fuproc.2007.11.003>

Mo, S., Li, S., Ren, Q., Zhang, M., Sun, Y., Wang, B. and Ye, D. 2018. Vertically-Aligned Co₃O₄ Arrays on Ni Foam as Monolithic Structured Catalysts for CO oxidation: Effects of Morphological Transformation. *Nanoscale*, 1-3: 7746–7758. <https://doi.org/10.1039/c8nr00147b>

Radwan, NRE., El-Shall, MS. and Hassan, HMA. 2007. Synthesis and Characterization of Nanoparticle Co₃O₄, CuO and NiO Catalysts Prepared by Physical and Chemical Methods to Minimize Air Pollution.

Applied Catalysis A: General, 331: 8–18. <https://doi.org/10.1016/j.apcata.2007.07.005>

Raghunath, CV. and Mondal, MK. 2017. Experimental Scale Multi Component Absorption of SO₂ and NO by NH₃/NaClO Scrubbing. Chemical Engineering Journal, 314: 537–547. <https://doi.org/10.1016/j.cej.2016.12.011>

Rosas, JM., Ruiz-Rosas, R., Rodríguez-Mirasol, J. and Cordero, T. 2017. Kinetic Study of SO₂ Removal Over Lignin-Based Activated Carbon. Chemical Engineering Journal, 307: 707–721. <https://doi.org/10.1016/j.cej.2016.08.111>

Sharma, M., Singh, J., Hazra, S. and Basu, S. 2017. Kinetic and Isotherm Studies on Adsorption of Toxic Pollutants using Porous ZnO@SiO₂ Monolith. Journal of Colloid Interface Science, 504: 669–679. <https://doi.org/10.1016/j.jcis.2017.06.020>

Singh, J., Bhunia, H. and Basu, S. 2018. Synthesis of Porous Carbon Monolith Adsorbents for Carbon Dioxide Capture: Breakthrough Adsorption Study. Journal of Taiwan Institute of Chemical Engineers, 89: 140–150. <https://doi.org/10.1016/j.jtice.2018.04.031>

Sousa, JPS., Pereira, MFR. and Figueiredo, JL. 2013. Modified Activated Carbon as Catalyst for NO Oxidation. Fuel Processing Technology, 106: 727–733. <https://doi.org/10.1016/j.fuproc.2012.10.008>

Sumathi, S., Bhatia, S., Lee, KT. and Mohamed, AR. 2009. Performance of an Activated Carbon Made from Waste Palm Shell in Simultaneous Adsorption of SO_x and NO_x of Flue Gas at Low Temperature. Science in China, Series E: Technology Science, 52: 198–203. <https://doi.org/10.1007/s11431-009-0031-6>

Sumathi, S., Bhatia, S., Lee, KT. and Mohamed, AR. 2010a. Cerium Impregnated Palm Shell Activated Carbon (Ce/PSAC) Sorbent for Simultaneous Removal of SO₂ and NO-Process Study. Chemical Engineering Journal, 162(1): 51–57. <https://doi.org/10.1016/j.cej.2010.04.056>

Sumathi, S., Bhatia, S., Lee, KT. and Mohamed, AR. 2010b. Selection of Best Impregnated Palm Shell Activated Carbon (PSAC) for Simultaneous Removal of SO₂ and NO_x. Journal of Hazardous Materials, 176(1-3): 1093–1096. <https://doi.org/10.1016/j.jhazmat.2009.11.037>

Teoh, YP., Khan, MA., and Choong, TSY. 2013. Kinetic and Isotherm Studies for Lead Adsorption from Aqueous Phase on Carbon Coated Monolith. Chemical Engineering Journal, 217: 248–255. <https://doi.org/10.1016/j.cej.2012.12.013>

Wu, D., Tan, Z., Yu, H., Li, Q., Thé, J. and Feng, X. 2016. Use of Nanofiltration to Reject Cobalt (II) from Ammoniacal Solutions Involved in Absorption of SO₂/NO_x. Chemical Engineering Science, 145: 97–107. <https://doi.org/10.1016/j.ces.2016.02.014>

Yi, H., Deng, H., Tang, X., Yu, Q., Zhou, X. and Liu, H. 2012. Adsorption Equilibrium and Kinetics for SO₂, NO, CO₂ on Zeolites FAU and LTA. Journal of Hazardous Materials, 203–204: 111–117. <https://doi.org/10.1016/j.jhazmat.2011.11.091>

Yin, Y., Wen, Z.H., Liu, X. Q., Yuan, AH. and Shi, L. 2018. Functionalization of SBA-15 with CeO₂ Nanoparticles for Adsorptive Desulfurization: Matters of Template P123. Adsorption Science and Technology 36(3-4): 953–966. <https://doi.org/10.1177/0263617417734767>

Zhang, H., Tong, H., Wang, S., Zhuo, Y., Chen, C. and Xu, C. 2006. Simultaneous Removal of SO₂ and NO from Flue Gas with Calcium-Based Sorbent at Low Temperature. Industrial Engineering and Chemistry Research, 45(18): 6099–6103. <https://doi.org/10.1021/ie060340e>

Zhao, Y., Hu, G., Sun, Z. and Yang, J. 2011. Simultaneous Removal of SO₂ and NO₂ on α -Al₂O₃ Absorbents Loaded with Sodium Humate and Ammonia Water. *Energy and Fuels*, 25(7): 2927–2931. <https://doi.org/10.1021/ef2002712>

Zhou, X., Yi, H., Tang, X., Deng, H. and Liu, H. 2012. Thermodynamics for the adsorption of SO₂, NO and CO₂ from flue gas on activated carbon fiber. *Chemical Engineering Journal*, 200–202: 399–404